Chapter 3

Hybrid Fault Diagnosis Method Based on Mechanical-Electrical Intersectional Characteristics for Generators

Yu-Ling He and Yue-Xin Sun

Additional information is available at the end of the chapter

http://dx.doi.org/10.5772/intechopen.79955

Abstract

In this chapter, a new hybrid fault diagnosis method based on the mechanical-electrical intersectional characteristics for turbo-generators is proposed. Different from other studies, this method not only employs the rotor vibration characteristics but also uses the stator vibration features and the circulating current properties inside the parallel branches of the same phase. Detailed theoretical analysis, as well as the experimental verification study, is carried out to demonstrate the proposed method. It is shown that in the proposed criterion for the method, the combining faulty characteristics for the single rotor eccentricity fault, the single rotor interturn short circuit fault, and the composite fault composed of the rotor eccentricity and the rotor interturn short circuit are all unique. The running conditions can be accurately and quickly identified by the proposed method. The work proposed in this chapter offers a new thought for the condition monitoring and the fault diagnosis of generators.

Keywords: turbo-generator, rotor eccentricity, rotor interturn short circuit, mechanical-electrical intersectional characteristics

1. Introduction

The generator is the key equipment for a power plant and needs timely and accurate monitoring and maintaining. Typically, after a long-term operation, generators may endure many electrical faults such as the rotor interturn short circuit (RISC) [1] and the stator interturn short circuit [2, 3], as well as mechanical faults such as rotor eccentricity [4].

RISC is the fault in which short circuit takes place between two adjacent turns inside the filed winding in the rotor [5]. That means, only the insulation between the two neighboring turns is damaged, while the main insulation of the whole winding bar is still fine.

Rotor eccentricity is the fault that occurs when the air-gap between the rotor and the stator is not average [6]. This fault can be further divided into three types, i.e., the static rotor eccentricity in which the minimum air-gap remains stable in a certain direction, the dynamic rotor eccentricity in which the minimum air-gap will vary as the rotor rotates, and the mixed rotor eccentricity in which static and the dynamic eccentricity occur at the same time. Generally, dynamic eccentricity is more complex and usually has a small eccentricity value, while static eccentricity is more common and more likely to have a larger eccentricity value caused by many factors such as bearing damage or un-accordance, assembling error, and deformation of the stator core. In this chapter, we mainly focus on the static rotor eccentricity.

So far, scholars have developed many monitoring and diagnosis methods for either the rotor eccentricity fault or the RISC fault. As for the rotor eccentricity fault, studies on the monitoring and diagnosis of air-gap eccentricity primarily focus on the stator current [7] and voltage [8, 9], the rotor current [9] and the shaft voltage [10], the inductance variation of the windings [11, 12], and the rotor UMP and vibration analysis [13–15]. The inductance variation analysis is mainly based on the winding function theory [16] and the improved winding function theory [17, 18] and needs a large amount of calculation, while the current and the voltage analysis is actually based on the harmonic changes of the magnetic flux density [7]. Using a direct analysis of the spectrum of the stator and rotor current or voltage obtained via Fourier transform, it is sometimes hard to exactly identify the eccentricity due to the inconspicuous amplitude changes compared with the noise signal magnitude, especially when the capacity of the generator is small or the eccentricity is not so severe. To overcome this disadvantage, scholars have developed an improved method using search coils [19].

People have studied the theoretical deduction and the simulation analysis of RISC in wind-powered generator [20, 21] and analyzed the change rate of the magnetic flux as well in order to detect this fault [22]. It is found that the induced voltage in rotor can be used to predict the location and the number of short circuit turns [23]. Meanwhile, researchers have also studied the characteristics of the excitation currents [24, 25], the copper losses [24], and the unbalanced magnetic pull (UMP) for the interturn short circuit monitoring [15, 26, 27]. Generally, at present, the application of search coils, which is mainly based on the magnetic field density (MFD) variation, is still adopted as a primary approach to monitor and diagnose this fault [28–30]. Therefore, further investigation on MFD variation characteristics at great length is of significance and will be the key to improve the monitoring level of the very failure. It is shown that some specific harmonic characteristics are very helpful and even more effective than other traditional means to diagnose the fault [31, 32].

However, since the actual performing condition is far more complex than the ideal normal condition and the single fault cases, the generator may display some untypical fault characteristics. For example, in addition to the RISC fault, the generator may have rotor eccentricity as well, i.e., the composite fault composed by rotor eccentricity and RISC. In this case, the fault characteristics are not the same as those of the single RISC fault or the single rotor eccentricity

fault. Thus the problem is to identify and diagnose the very fault (the single rotor eccentricity, the single RISC, and the composite fault) accurately.

In this chapter, we will discuss a new method combining the mechanical fault characteristics, i.e., the stator and the rotor vibration characteristics, with the electrical fault characteristics, i.e., the circulating current inside the parallel branches of the same phase (CCPB), to identify the single rotor eccentricity fault, the single RISC fault, and the composite fault composed by these two.

2. Theoretical analysis

As is widely comprehended, the electrical and the mechanical properties of the generator are all closely related to the magnetic flux density (MFD). For example, the magnetic pulls acting on the stator core and the rotor core are in proportion to the square of MFD, and the stator current and voltage are in direct proportion to MFD. Generally, both the rotor eccentricity fault and the RISC fault will affect MFD.

In this section, we will firstly analyze the impact of the four running conditions, i.e., the normal condition, the single rotor eccentricity fault, the single RISC fault, and the composite fault composed of rotor eccentricity and RISC. Then, the unbalanced magnetic pull (UMP) formulas and the electromotive force difference expression between the two parallel branches will be deduced in detail to obtain the qualitative theoretical results.

2.1. MFD study for each case

MFD is composed by two factors, the magnetomotive force (MMF) and the permeance per unit area. Usually MFD is written as

$$B(\alpha_m, t) = f(\alpha_m, t)\Lambda(\alpha_m, t) \tag{1}$$

where $f(\alpha_m, t)$ is the MMF, and $\Lambda(\alpha_m, t)$ is the permeance per unit area.

Typically, RISC primarily affects MMF but has little impact on the permeance, while the rotor eccentricity mainly impacts on the permeance per unit area but has little influence on MMF. In normal condition, there is neither RISC nor rotor eccentricity. In this case, the air-gap can be indicated as **Figure 1(a)**, while the rotor MMF and the vector diagram of the stator and rotor MMFs can be indicated as given in **Figure 2(a)** and **Figure 3(a)**, respectively, by the shorted turns.

As indicated in **Figure 3(a)**, the MMF in normal condition can be written as

$$\begin{cases} f(\alpha_m, t) = F_r \cos(\omega t - \alpha_m) + F_s \cos\left(\omega t - \alpha_m - \dfrac{\pi}{2} - \psi\right) = F_1 \cos(\omega t - \alpha_m - \beta) \\ F_1 = \sqrt{(F_r - F_s \sin\psi)^2 + (F_s \cos\psi)^2} \\ \beta = \arctan\dfrac{F_s \cos\psi}{F_r - F_s \sin\psi} \end{cases} \tag{2}$$

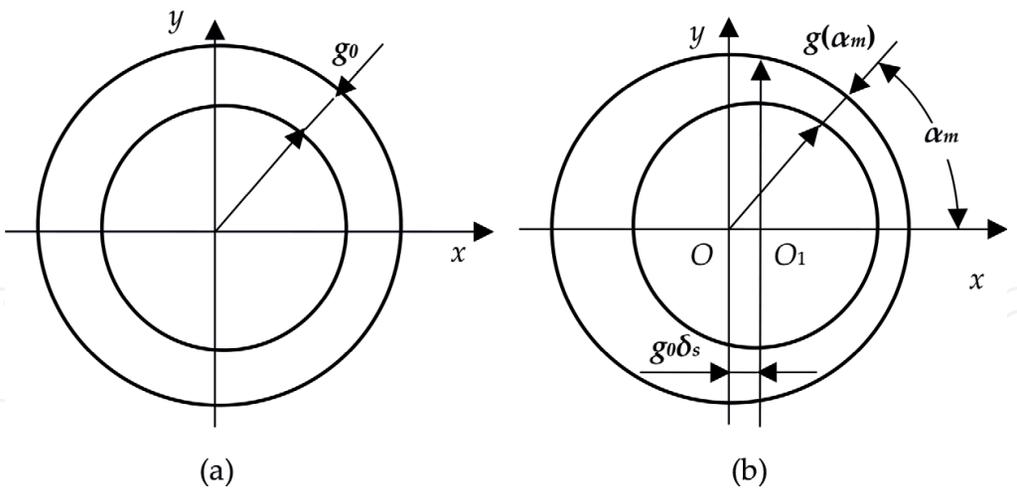

Figure 1. Air-gap for the four performing conditions. (a) Normal condition and RISC and (b) rotor eccentricity and composite fault.

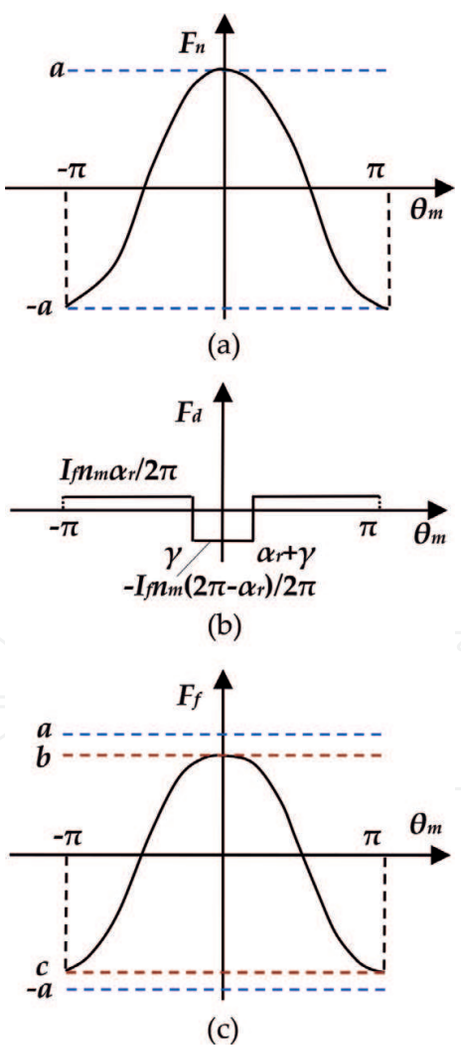

Figure 2. Rotor MMF before and after RISC. (a) Normal rotor MMF, (b) inverse MMF produced, and (c) MMF under RISC.

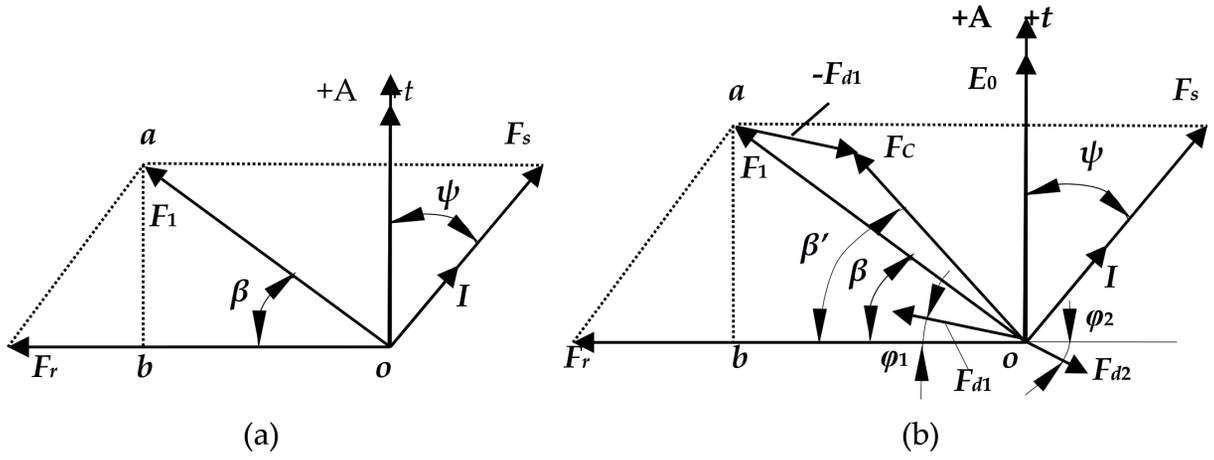

Figure 3. Vector diagram of the stator and rotor MMFs for the four performing conditions. (a) Normal condition and rotor eccentricity and (b) RISC and composite fault.

Since the permeance per unit area is in inverse proportion to the radial air-gap length, the permeance per unit area in normal condition can be written as

$$\Lambda(\alpha_m, t) = \frac{\mu_0}{g(\alpha_m, t)} = \frac{\mu_0}{g_0} = \Lambda_0 \tag{3}$$

In the case of rotor eccentricity, the MMF is the same as in normal condition, while the permeance per unit area is

$$\begin{cases} \Lambda(\alpha_m, t) = \dfrac{\mu_0}{g(\alpha_m, t)} = \dfrac{\mu_0}{g_0(1 - \delta_s \cos\alpha_m)} = \dfrac{\mu_0}{g_0}\left(1 + \delta_s \cos\alpha_m + \delta_s^2 \cos^2\alpha_m + \cdots\right) \\ \qquad\qquad \approx \Lambda_0(1 + \delta_s \cos\alpha_m) = \Lambda_0 + \Lambda_s \cos\alpha_m \\ \Lambda_s = \Lambda_0 \delta_s \end{cases} \tag{4}$$

where μ_0 is the permeability of the air, g_0 is the radial air-gap length, and δ_s is the relative rotor eccentricity.

In the case of RISC, since there is no longer exciting current in the shorted turns, it is equivalent to adding an inverse current to the normal exciting current for the shorted turns. The rotor MMF before and after RISC is indicated in **Figure 2**. Since the area of the produced positive MMF should be equal to that of the induced negative MMF, the inverse MMFs produced by the shorted turns can be written as

$$f_d(\theta_m) = \begin{cases} -\dfrac{I_f n_m (2\pi - \alpha_r)}{2\pi} & \gamma \le \theta_m \le \gamma + \alpha_r \\ \dfrac{I_f n_m \alpha_r}{2\pi} & \textit{other condition} \end{cases} \tag{5}$$

where θ_m is the circumferential angle on the rotor surface, I_f is the exciting current of the generator, n_m is the number of the shorted turns, γ is the circumferential angle to indicate the beginning RISC position, and α_r is the angle between the two slots where RISC takes place.

$F_d(\theta_m)$ can be expanded by Fourier series and written as

$$\begin{cases} f_d(\theta_m) = A_0 + \sum_{n=1}^{\infty}[A_n \cos(n\theta_m) + B_n \sin(n\theta_m)] \\ A_0 = \frac{1}{2\pi}\int_0^{2\pi} F_d(\theta_m)d\theta_m = 0 \\ A_n = \frac{1}{\pi}\int_0^{2\pi} F_d(\theta_m)\cos(n\theta_m)d\theta_m = -\frac{I_f n_m[\sin(n(\alpha_r+\gamma)) - \sin(n\gamma)]}{n\pi} \\ B_n = \frac{1}{\pi}\int_0^{2\pi} F_d(\theta_m)\sin(n\theta_m)d\theta_m = \frac{I_f n_m[\cos(n(\alpha_r+\gamma)) - \cos(n\gamma)]}{n\pi} \end{cases} \tag{6}$$

Since the nth MMF harmonic is equivalent to the main MMF which is produced by the generator that has n pole-pairs, the reverse MMF induced by the short circuit turns can be written as a function which is both time and space dependent.

$$\begin{cases} F_d(\alpha_m, t) = \sum_{n=1}^{\infty}[A_n \cos n(\omega t - \alpha_m) + B_n \sin n(\omega t - \alpha_m)] = \sum_{n=1}^{\infty} F_{dn} \cos n(\omega t - \alpha_m - \varphi_n) \\ F_{dn} = \sqrt{{A_n}^2 + {B_n}^2} \\ \varphi_n = \arctan\frac{B_n}{A_n} \end{cases} \tag{7}$$

Correspondingly, ignoring the higher-order harmonics, according to **Figure 3(b)**, the MMF under RISC can be written as

$$\begin{cases} f(\alpha_m, t) = F_1 \cos(\omega t - \alpha_m - \beta) - F_{d1}\cos(\omega t - \alpha_m - \varphi_1) - F_{d2}\cos(\omega t - \alpha_m - \pi - \varphi_2) \\ \qquad = F_C \cos\cos(\omega t - \alpha_m - \beta') - F_{d2}\cos(\omega t - \alpha_m - \pi - \varphi_2) \\ F_C = \sqrt{(F_r - F_s\sin\psi - F_{d1}\cos\varphi_1)^2 + (F_s\cos\psi - F_{d1}\sin\varphi_1)^2} \\ \beta' = \arctan\frac{F_s\cos\psi - F_{d1}\sin\varphi_1}{F_r - F_s\sin\psi - F_{d1}\cos\varphi_1} \end{cases} \tag{8}$$

Feeding Eqs. (2)–(4) and (8) into (1), the MFDs for the four running conditions can be obtained.

$$B(\alpha_m, t) = \begin{cases} F_1\cos(\omega t - \alpha_m - \beta)\Lambda_0 \cdots\cdots\cdots\cdots\cdots\cdots\cdots\cdots\cdots\cdots\cdots\cdots\text{normal} \\ F_1\cos(\omega t - \alpha_m - \beta)(\Lambda_0 + \Lambda_s\cos\alpha_m) \cdots\cdots\cdots\cdots\cdots\cdots\cdots\text{rotor eccentricity} \\ [F_C\cos\cos(\omega t - \alpha_m - \beta') - F_{d2}\cos(\omega t - \alpha_m - \pi - \varphi_2)]\Lambda_0 \cdots\cdots\cdots\text{RISC} \\ [F_C\cos\cos(\omega t - \alpha_m - \beta') - F_{d2}\cos(\omega t - \alpha_m - \pi - \varphi_2)] \\ \quad \times(\Lambda_0 + \Lambda_s\cos\alpha_m) \qquad \cdots\cdots\cdots\text{composite fault} \end{cases} \tag{9}$$

2.2. Mechanical-electrical characteristic analysis

The physical model of the stator core is a hollow shell, as indicated in **Figure 4**, while the physical model of the rotor core is the rigid cylinder. Therefore, the essential exciting force for the stator core is the magnetic pull per unit area (MPPUA), while for the rotor it is the integral

http://dx.doi.org/10.5772/intechopen.79955

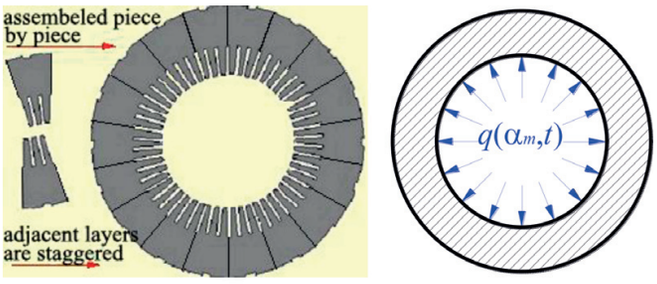

Figure 4. Structure and magnetic force of stator core. (a) Structure of stator core and (b) MPPUA on stator core.

force. This may not be easy to understand, but it can be suggested from **Figure 4(b)** that though the integral force of the stator core is zero due to the symmetric distribution of the unit force, it will still have periodical shrinking-expanding deformations, i.e., the radial vibrations, due to the cyclical pulsating feature of the MPPUA. However, for the rotor core, the MPPUA is not enough to cause radial vibrations for this solid cylinder. Therefore, the internal force, i.e., the unbalanced magnetic pull (UMP) will be the essential exciting force for the rotor.

The MPPUA and the UMP can be calculated via

$$\begin{cases} q(\alpha_m,t) = \dfrac{[B(\alpha_m,t)]^2}{2\mu_0} & \text{MPPUA} \\ \begin{cases} F_X = LR\displaystyle\int_0^{2\pi} q(\alpha_m,t)\cos\alpha_m d\alpha_m \\ F_Y = LR\displaystyle\int_0^{2\pi} q(\alpha_m,t)\sin\alpha_m d\alpha_m \end{cases} & \text{UMP} \end{cases} \tag{10}$$

Feeding Eq. (9) into (10), the exciting force needed to cause stator vibration and rotor vibration can be, respectively, written as Eqs. (11) and (12).

Since the stator and rotor vibration will have the same frequency harmonic components as the exciting force, as indicated in Eq. (11), the stator will have second harmonic vibrations in normal condition and in the rotor eccentricity case, while it will have first, second, third, and fourth harmonic components under RISC and the composite fault. Obviously, it is hard to identify the fault type accurately only by means of the stator vibration.

Comparing MPPUA formulas in the four running conditions in Eq. (11), it can be found that the magnitude of the second harmonic under rotor eccentricity fault will be larger than that of the normal condition because extra second harmonic terms are added in the formula. However, the magnitude of the second harmonic MPPUA under RISC will be smaller than that in normal condition because F_C is smaller than F_1, see **Figure 3(b)**. For the composite fault, the second harmonic MPPUA magnitude will be smaller than that under rotor eccentricity but larger than that in the RISC case. Since there is theoretically no fourth harmonic in normal condition when only considering the first MMFs, the occurrence of RISC will increase the fourth harmonic MPPUA.

The rotor, as indicated in Eq. (12), will have no vibrations in normal condition, while it will endure second harmonic vibrations in the case of rotor eccentricity; first harmonic vibration under RISC; and first, second, and third harmonic vibrations under the composite fault. It seems that the four running conditions can be identified by the rotor vibration characteristics. However, still other faults have the same rotor vibration features, leading to practical difficulties for exact diagnosis. For example, the mass imbalance fault will also cause the rotor to vibrate at the fundamental frequency, and the shaft misalignment fault will also lead to the rotor's second harmonic vibrations. Therefore, it is actually still hard to diagnose the fault accurately by only using the rotor vibration properties.

In fact, in addition to the stator and rotor vibrations, the circulating current inside the parallel branches (CCPB) of the same phase will vary as well due to different running conditions. Taking the SDF-9 type generator which will be employed as the study object behind as an example, the parallel branches and the CCPB in Phase A are indicated in **Figure 5**.

$$
q(\alpha_m,t)=\begin{cases}
\dfrac{{F_1}^2}{8\mu_0}\left[2\Lambda_0^2+2\Lambda_0^2\cos\left(2\omega t-2\alpha_m-2\beta\right)\right]\ldots\ldots\text{normal condition}\\
\dfrac{{F_1}^2}{8\mu_0}\Big\{\left[\left(2\Lambda_0^2+\Lambda_s^2\right)+\left(4\Lambda_0\Lambda_s\cos\alpha_m\right)+\left(\Lambda_s^2\cos 2\alpha_m\right)\right]\\
\quad+\left[0.5\Lambda_s^2\cos\left(2\omega t-2\beta\right)+2\Lambda_0\Lambda_s\cos\left(2\omega t-\alpha_m-2\beta\right)\right.\\
\quad+\left(2\Lambda_0^2+\Lambda_s^2\right)\cos\left(2\omega t-2\alpha_m-2\beta\right)+2\Lambda_0\Lambda_s\cos\left(2\omega t-3\alpha_m-2\beta\right)\\
\quad\left.+0.5{\Lambda_s}^2\cos\left(2\omega t-4\alpha_m-2\beta\right)\right]\Big\}\ldots\ldots\text{rotor eccentricity}\\
\dfrac{\Lambda_0^2}{4\mu_0}\left[F_C^2+F_{d2}^2-2F_CF_{d2}\cos\left(\omega t-\alpha_m+\beta_1-2\varphi_2\right)\right.\\
\quad+F_C^2\cos 2\left(\omega t-\alpha_m-\beta\right)-2F_CF_{d2}\cos\left(3\omega t-3\alpha_m-\beta_1-2\varphi_2\right)\\
\quad\left.+F_{d2}^2\cos 4\left(\omega t-\alpha_m-\varphi_2\right)\right]\ldots\ldots\text{RISC}\\
\dfrac{1}{8\mu_0}\Big\{\left[\left(F_C^2+F_{d2}^2\right)\left(2\Lambda_0^2+\Lambda_s^2\right)+4\left(F_C^2+F_{d2}^2\right)\Lambda_0\Lambda_s\cos\alpha_m+\left(F_C^2+F_{d2}^2\right)\Lambda_s^2\cos 2\alpha_m\right]\\
\quad+\left[-4F_CF_{d2}\Lambda_0\Lambda_s\cos\left(\omega t+\beta_1-2\varphi_2\right)-2F_CF_{d2}\left(2\Lambda_0^2+\Lambda_s^2\right)\cos\left(\omega t-\alpha_m+\beta_1-2\varphi_2\right)\right.\\
\quad-F_CF_{d2}\Lambda_s^2\cos\left(\omega t+\alpha_m+\beta_1-2\varphi_2\right)-4F_CF_{d2}\Lambda_0\Lambda_s\cos\left(\omega t-2\alpha_m+\beta_1-2\varphi_2\right)\\
\quad\left.-F_CF_{d2}\Lambda_s^2\cos\left(\omega t-3\alpha_m+\beta_1-2\varphi_2\right)\right]+\left[0.5F_C^2\Lambda_s^2\cos\left(2\omega t-2\beta_1\right)\right.\\
\quad+2F_C^2\Lambda_0\Lambda_s\cos\left(2\omega t-\alpha_m-2\beta_1\right)+F_C^2\left(2\Lambda_0^2+\Lambda_s^2\right)\cos\left(2\omega t-2\alpha_m-2\beta_1\right)\\
\quad+2F_C^2\Lambda_0\Lambda_s\cos\left(2\omega t-3\alpha_m-2\beta_1\right)+0.5F_C^2\Lambda_s^2\cos\left(2\omega t-4\alpha_m-2\beta_1\right)\left.\right]\\
\quad+\left[-F_CF_{d2}\Lambda_s^2\cos\left(3\omega t-\alpha_m-\beta_1-2\varphi_2\right)-4F_CF_{d2}\Lambda_0\Lambda_s\cos\left(3\omega t-2\alpha_m-\beta_1-2\varphi_2\right)\right.\\
\quad-2F_CF_{d2}\left(2\Lambda_0^2+\Lambda_s^2\right)\cos\left(3\omega t-3\alpha_m-\beta_1-2\varphi_2\right)\\
\quad\left.-4F_CF_{d2}\Lambda_0\Lambda_s\cos\left(3\omega t-4\alpha_m-\beta_1-2\varphi_2\right)-F_CF_{d2}\Lambda_s^2\cos\left(3\omega t-5\alpha_m-\beta_1-2\varphi_2\right)\right]\\
\quad+\left[0.5F_{d2}^2\Lambda_s^2\cos\left(4\omega t-2\alpha_m-4\varphi_2\right)+2F_{d2}^2\Lambda_0\Lambda_s\cos\left(4\omega t-3\alpha_m-4\varphi_2\right)\right.\\
\quad+F_{d2}^2\left(2\Lambda_0^2+\Lambda_s^2\right)\cos\left(4\omega t-4\alpha_m-4\varphi_2\right)+2F_{d2}^2\Lambda_0\Lambda_s\cos\left(4\omega t-5\alpha_m-4\varphi_2\right)\\
\quad\left.+0.5F_{d2}^2\Lambda_s^2\cos\left(4\omega t-6\alpha_m-4\varphi_2\right)\right]\Big\}\ldots\ldots\text{composite fault}
\end{cases}
\tag{11}
$$

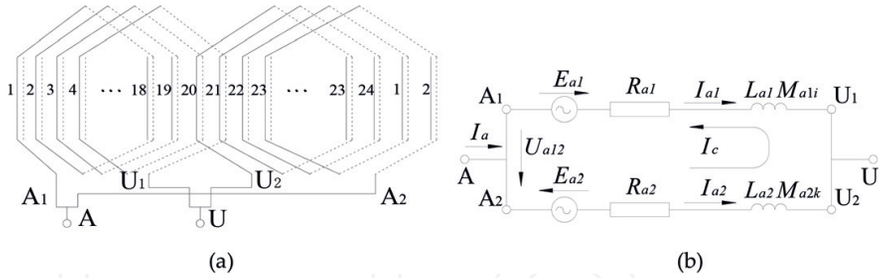

Figure 5. Parallel branch and CCPB in Phase A. (a) Winding distribution of Phase A and (b) equal circuit of parallel branches of Phase A.

The electromotive force difference between the two branches, which is indicated in **Figure 5(b)** and is the exciting source of the CCPB, can be obtained via Eq. (13), where E_{a1} and E_{a2} are the electromotive forces of the two branches, respectively; q is the number of slots for each pole per phase; w_c is the number of turns for each branch winding; k_{w1} is the fundamental frequency winding factor; τ is the polar distance; l is the effective length of the winding; and f is the electrical frequency. Feeding Eq. (9) into (13), the electromotive force difference can be obtained and written as in Eq. (14).

As indicated in Eq. (14), the CCPB has different features due to varied running conditions. However, it has the similar problem as the rotor vibration while using it as the fault diagnosis criterion. For example, due to the initial asymmetry inside the generator, the generator may have first harmonic CCPB in normal condition. Consequently, the CCPB features will be very similar not only between normal condition and rotor eccentricity, but also between RISC and the composite fault. Thus, it is still not enough to only use CCPB difference to identify the faults accurately.

$$
\begin{cases}
\left.\begin{aligned} F_X &= LR\int_0^{2\pi} q(\alpha_m,t)\cos\alpha_m d\alpha_m = 0 \\ F_Y &= LR\int_0^{2\pi} q(\alpha_m,t)\sin\alpha_m d\alpha_m = 0 \end{aligned}\right\}\text{.....normal condition} \\
\left.\begin{aligned} F_X &= \frac{LRF_1^2\pi}{4\mu_0}\left[2\Lambda_0\Lambda_s + 2\Lambda_0\Lambda_d\cos\omega t + \Lambda_0\Lambda_d\cos\left(\omega t - 2\beta\right)\right. \\ &\quad \left.+\Lambda_0\Lambda_s\cos\left(2\omega t - 2\beta\right)\right] \\ F_Y &= \frac{LRF_1^2\pi}{4\mu_0}\left[2\Lambda_0\Lambda_d\sin\omega t + \Lambda_0\Lambda_d\sin\left(\omega t - 2\beta\right)\right. \\ &\quad \left.+\Lambda_0\Lambda_s\sin\left(2\omega t - 2\beta\right)\right] \end{aligned}\right\}\text{.....rotor eccentricity} \\
\left.\begin{aligned} F_X &= LR\int_0^{2\pi} q(\alpha_m,t)\cos\alpha_m d\alpha_m = \frac{-F_C F_{d2} LR\Lambda_0^2\pi}{2\mu_0}\cos\left(\omega t + \beta_1 - 2\varphi_2\right) \\ F_Y &= LR\int_0^{2\pi} q(\alpha_m,t)\sin\alpha_m d\alpha_m = \frac{-F_C F_{d2} LR\Lambda_0^2\pi}{2\mu_0}\sin\left(\omega t + \beta_1 - 2\varphi_2\right) \end{aligned}\right\}\text{.....RISC} \\
\left.\begin{aligned} F_X &= \frac{LR\pi}{8\mu_0}\left\{\left[4\left(F_C{}^2 + F_{d2}{}^2\right)\Lambda_0\Lambda_s\right]\right. \\ &\quad +\left[-2F_C F_{d2}\left(2\Lambda_0^2 + 1.5\Lambda_s^2\right)\cos\left(\omega t + \beta_1 - 2\varphi_2\right)\right] \\ &\quad \left.+\left[2F_C^2\Lambda_0\Lambda_s\cos\left(2\omega t - 2\beta_1\right)\right] - \left[F_C F_{d2}\Lambda_s^2\cos\left(3\omega t - \beta_1 - 2\varphi_2\right)\right]\right\} \\ F_Y &= \frac{LR\pi}{8\mu_0}\left\{\left[-2F_C F_{d2}\left(2\Lambda_0^2 + 0.5\Lambda_s^2\right)\sin\left(\omega t + \beta_1 - 2\varphi_2\right)\right]\right. \\ &\quad \left.+\left[2F_C^2\Lambda_0\Lambda_s\sin\left(2\omega t - 2\beta_1\right)\right] - \left[F_C F_{d2}\Lambda_s^2\sin\left(3\omega t - \beta_1 - 2\varphi_2\right)\right]\right\} \end{aligned}\right\}\text{..compostie fault}
\end{cases}
\tag{12}
$$

$$\begin{cases} U_{a12}(\alpha_m, t) = -E_{a1}(\alpha_m, t) + j\omega L_{a1} I_{a1} + R_{a1} I_{a1} + j\omega \sum_i M_{a1i} I_i \\ \qquad\qquad -j\omega \sum_k M_{a2k} I_k - R_{a2} I_{a2} - j\omega L_{a2} I_{a2} - E_{a2}(\alpha_m, t) \\ E_{a1}(\alpha_m, t) = 2qw_c k_{w1} \tau l f B(\alpha_m, t) \\ E_{a2}(\alpha_m, t) = 2qw_c k_{w1} \tau l f B[(\alpha_m - \pi), t] \end{cases} \tag{13}$$

$$U_{a12} = \begin{cases} 0 \cdot \cdots\cdots\cdots\cdots\cdots\cdots\cdots\cdots\cdots\cdots\cdots\cdots\text{normal condition} \\ -4qw_c k_{w1} \tau l f F_1 \Lambda_s \cos\alpha_m \cos\left(\omega t - \alpha_m - \beta\right) \cdot \cdots\cdots\text{rotor eccentricity} \\ 4qw_c k_{w1} \tau l f F_{d2} \Lambda_0 \cos 2\left(\omega t - \alpha_m - \varphi_2\right) \cdot \cdots\cdots\cdots\cdots\cdots\cdots\text{RISC} \\ 2qw_c k_{w1} \tau l f [F_C \Lambda_s \cos\left(\omega t - \beta_1\right) + F_C \Lambda_s \cos\left(\omega t - 2\alpha_m - \beta_1\right) \\ \quad - F_{d2} \Lambda_0 \cos 2\left(\omega t - \alpha_m - \varphi_2\right)] \cdots\cdots\cdots\cdots\cdots\text{composite fault} \end{cases} \tag{14}$$

3. Hybrid diagnosis method and verification

3.1. Method description

Based on the previously described theoretical study, a hybrid diagnosis method combining the mechanical characteristics, i.e., the stator and the rotor vibration characteristics, with the electrical features, i.e., the CCPB properties, can be proposed, as shown in **Table 1**.

As indicated in **Table 1**, the combining mechanical-electrical intersectional fault characteristics are unique for each fault. It will be obviously more advantageous than only employing either the vibration or the CCPB characteristics.

Running condition	Stator vibration	Rotor vibration	CCPB
Normal condition	2nd harmonic	—	—
Rotor eccentricity	2nd harmonic	2nd harmonic	1st harmonic
RISC	1st, 2nd, 3rd, 4th harmonics, comparing with normal condition, the 2nd decreased while 1st, 3rd, and 4th increased	1st harmonic	2nd harmonic
Composite fault	1st, 2nd, 3rd, and 4th harmonics, comparing with normal condition, the 1st, 3rd, and 4th increased	1st, 2nd, and 3rd harmonics	1st and 2nd harmonics

Table 1. Detailed criteria of the hybrid diagnosis method.

3.2. Experimental verification

The experimental verification is taken on a SDF-9 type fault simulating generator, in the National Key Lab of New Energy Electric Power System, P.R. China, as indicated in **Figure 6(a)**. The primary parameters of the generator are shown in **Table 2**.

http://dx.doi.org/10.5772/intechopen.79955

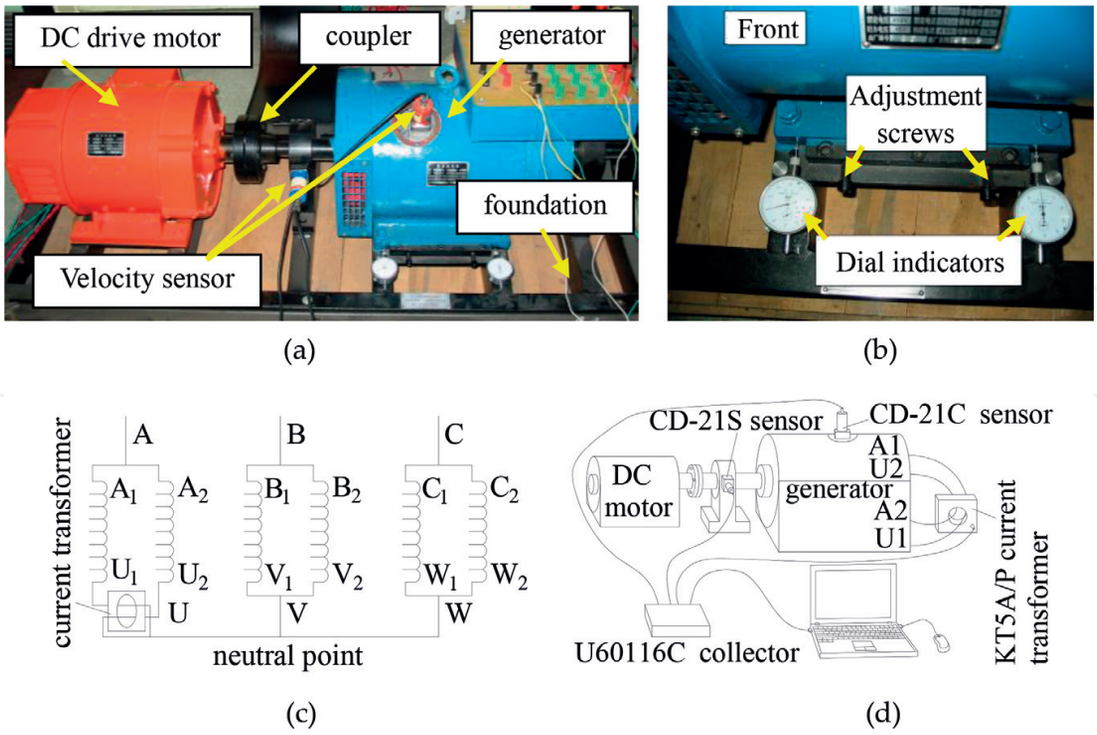

Figure 6. Experiment method of the fault simulating generator. (a) General outlook, (b) method to set rotor eccentricity, (c) method to test CCPB and (d) testing system of the experiment.

Parameters	Values
Rated capacity	7.5 kVA
Rated exciting current	1.5 A
Rated rotation speed	3000 r/min
Number of pole pairs	$p = 1$
Polar distance	$\tau = 252$ mm
Radial air-gap length	$g_0 = 0.8$ mm
Number of exciting slots per pole	6
Number of exciting turns peer pole	480
Number of stator slots	24
Number of turns in series per phase	100
Ratio of pitch to polar distance	$k_y = y/\tau = 0.83$
Pitch shortening factor	$k_p = 0.966$

Table 2. Primary parameters of study object.

The rotor of the generator is kept to the underframe by the bearing pedestal, while the stator can be moved along the horizontally radial direction by adjusting the screws; see **Figure 6(b)**. The movement can be controlled by two dial indicators, so that different fault degrees of rotor eccentricity can be simulated.

During the experiment, two velocity sensors are employed to test the stator vibration and the rotor vibration (see **Figure 6a**), while the CCPB is measured by a current transformer (see **Figure 6c**, the conductors of the two branches inversely cross the current transformer to get the current difference which is also the CCPB). The tested data are collected by a U60116C type collector and stored in the computer; see **Figure 6(d)**.

The stator vibration spectra for the four running conditions are indicated in **Figure 7**, while the rotor vibration spectra and the CCPB spectra for each performing case are illustrated in **Figures 8** and **9**, respectively. Theoretically, in normal condition, the stator should have only the second harmonic vibration component, and there should be no rotor vibrations or circulating currents. However, the experimental data show some differences. This is mainly caused by the asymmetry inside the generator. For example, the winding distribution in the generator may not be strictly symmetric. These initial values which should be zero in theory can be treated as the null drift of the generator system.

As indicated in **Figure 7**, it is shown that the four performing conditions will have different stator vibration characteristics. The occurrence of the rotor eccentricity will obviously increase the amplitude of the second harmonic, while the occurrence of RISC will decrease this

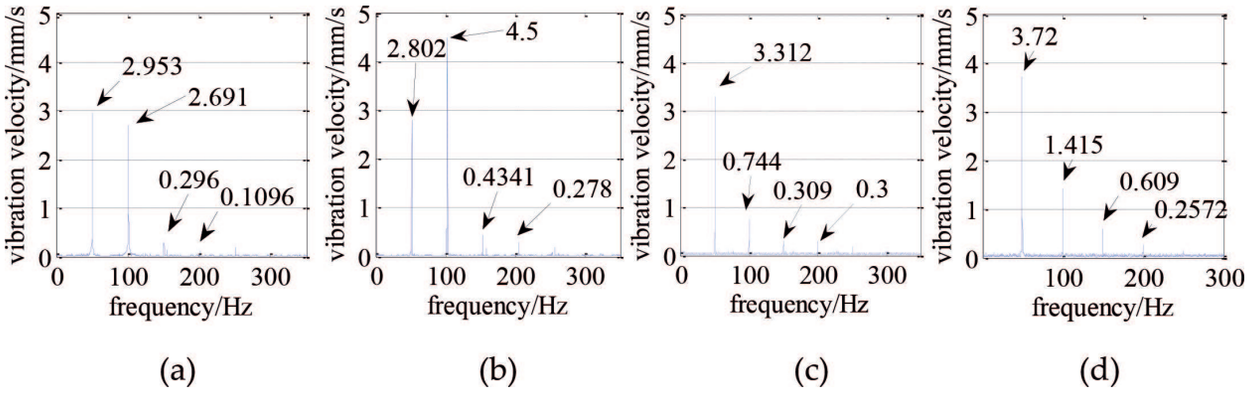

Figure 7. Stator vibration spectra under different conditions. (a) Normal condition, (b) 0.3 mm eccentricity, (c) 3% RISC and (d) composite fault.

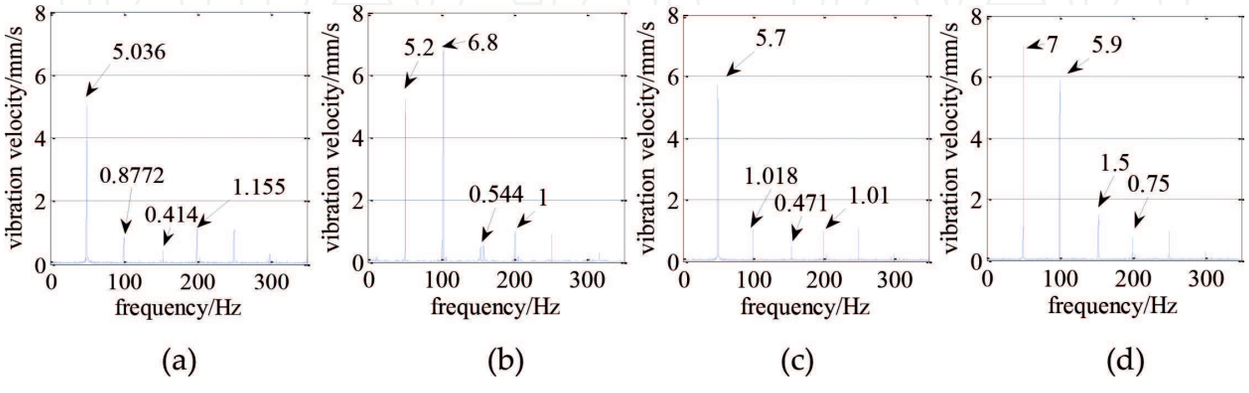

Figure 8. Rotor vibration spectra under different conditions. (a) Normal condition, (b) 0.3 mm eccentricity, (c) 3% RISC and (d) composite fault.

http://dx.doi.org/10.5772/intechopen.79955

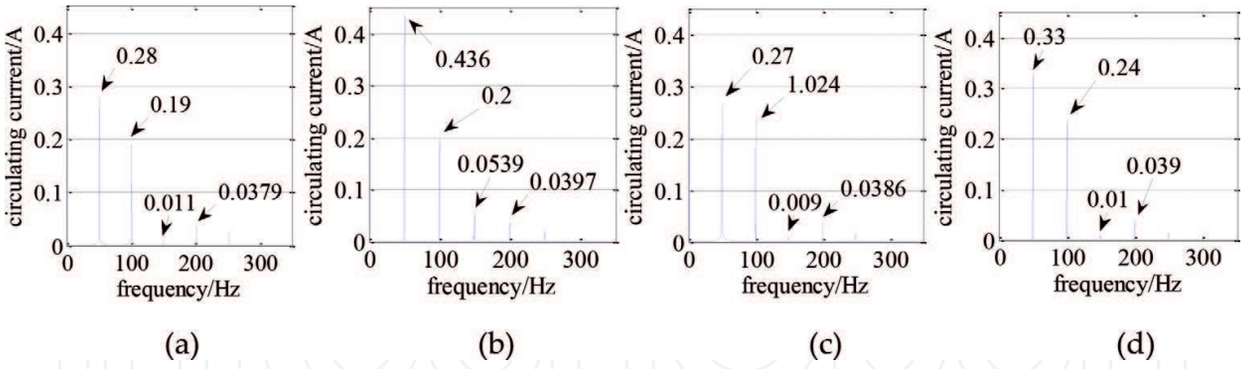

Figure 9. CCPB spectra under different conditions. (a) Normal condition, (b) 0.3 mm eccentricity, (c) 3% RISC and (d) composite fault.

harmonic but increase the first, third, and fourth harmonics. For the composite fault, the amplitude of the second harmonic is generally between the rotor eccentricity and RISC. The experimental results are consistent with the previously described theoretical analysis.

As indicated in **Figure 8**, the second harmonic vibration amplitude will be increased as the rotor eccentricity takes place, while the occurrence of RISC will increase the first harmonic amplitude. In the case of the composite fault, comparing with the normal condition, all of the first, second, and third harmonic amplitudes will be increased. This tendency to develop harmonic amplitude is in accordance with the theoretical result.

As indicated in **Figure 9**, the rotor eccentricity will mainly increase the first harmonic CCPB, while RISC will primarily increase the second harmonic CCPB. In the case of the composite fault, both the first and the second harmonic amplitudes of the CCPB will be enlarged. This experimental result still follows that of the previous theoretical study.

It is suggested from **Figures 7–9** that the stator vibration, the rotor vibration, and the CCPB will all vary due to different performing conditions. Combining the stator and the rotor vibration characteristics with the CCPB varying features, the mentioned four running conditions can be effectively and accurately identified. To confirm this, we have also carried out the experiments several times. And, by using the hybrid method proposed in this chapter, we correctly identified the running conditions each time.

4. Conclusions

In this chapter, we propose a new hybrid fault diagnosis method based on the intersectional mechanical-electrical characteristics. Primary conclusions drawn from the study are as follows.

1. Given the complex practical running condition, it is hard to identify the fault accurately only by either the stator vibration characteristics or the rotor vibration features.
2. In addition to the rotor and the stator vibration characteristics, the circulating current inside the parallel branches of the same phase is also an effective tool for condition monitoring and fault diagnosis.

3. By combining the rotor and stator vibration characteristics with the circulating current inside the parallel branches, the four running conditions, i.e., the normal condition, the single rotor eccentricity fault, the rotor interturn short circuit fault, and the composite fault composed of the rotor eccentricity and the rotor interturn short circuit, can be accurately identified due to the unique combining fault characteristics.

Acknowledgements

This work was in part supported by National Natural Science Foundation of China (51777074, 51307058), Natural Science Foundation of Hebei Province, China (E2015502013), and Chinese Fundamental Research Funds for the Central Universities (2018YQ03).

Conflict of interest

There is no conflict of interest regarding the publication of this work.

Author details

Yu-Ling He* and Yue-Xin Sun

*Address all correspondence to: heyuling1@163.com

Department of Mechanical Engineering, North China Electric Power University, Baoding, Hebei, China

References

[1] He Y-L, Ke M-Q, Tang G-J, Jiang H-C, Yuan X-H. Analysis and simulation on the effect of rotor interturn short circuit on magnetic flux density of turbo-generator. Journal of Electrical Engineering—Elektrotechnicky Casopis. 2016;**67**:323-333. DOI: 10.1515/jee-2016-0047

[2] Gandhi A, Corrigan T, Parsa L. Recent advances in modeling and online detection of stator interturn faults in electrical motors. IEEE Transactions on Industrial Electronics. 2011;**58**: 1564-1575. DOI: 10.1109/TIE.2010.2089937

[3] He Y-L, Wang F-L, Tang G-J, Ke M-Q. Analysis on steady-state electromagnetic characteristics and online monitoring method of stator inter-turn short circuit of turbo-generator. Electric Power Components and Systems. 2017;**45**:198-210. DOI: 10.1080/15325008.2016.1247387

[4] Tang G-J, Ke M-Q, He Y-L, Wang F-L. United electromagnetic characteristics and online monitoring method of static air-gap eccentricity of turbo-generator. Journal of Electrical Engineering and Technology. 2016;**11**:1614-1627. DOI: 10.5370/JEET.2016.11.6.1614

[5] Hao L, Wu J, Zhou Y. Theoretical analysis and calculation model of the electromagnetic torque of nonsalient-pole synchronous machines with interturn short circuit in field windings. IEEE Transactions on Energy Conversion. 2015;**30**:110-121. DOI: 10.1109/TEC.2014.2350336

[6] He Y-L, Deng W-Q, Tang G-J. Impact of different static air-gap eccentricity forms on rotor UMP of turbogenerator. Mathematical Problems in Engineering. 2016;**2016**:1-13. https://www.hindawi.com/journals/mpe/2016/5284815/cta/. Open Access. DOI: 10.1155/2016/5284815

[7] Bruzzese C. Diagnosis of eccentric rotor in synchronous machines by analysis of split-phase currents—Part II: Experimental analysis. IEEE Transactions on Industrial Electronics. 2014;**61**:4206-4216. DOI: 10.1109/TIE.2013.2284554

[8] Zhu J-h, A-rui Q, Guo T. Branch voltage of a salient pole synchronous generator with eccentric rotor and skewed slots. Journal of Tsinghua University (Science and Technology). 2008;**48**:453-456

[9] Bruzzese C, Joksimovic G. Harmonic signatures of static eccentricities in the stator voltages and in the rotor current of no-load salient-pole synchronous generators. IEEE Transactions on Industrial Electronics. 2011;**58**:1606-1624. DOI: 10.1109/TIE.2010.2087296

[10] Doorsamy W, Abdallh AAE, Cronje WA, Dupré L. An experimental design for static eccentricity detection in synchronous machines using a Cramér–Rao lower bound technique. IEEE Transactions on Energy Conversion. 2015;**30**:254-261. DOI: 10.1109/TEC.2014.2347895

[11] Iamamura BAT, Le Menach Y, Tounzi A, Sadowski N, Guillot E. Study of static and dynamic eccentricities of a synchronous generator using 3-D FEM. IEEE Transactions on Magnetics. 2010;**46**:3516-3519. DOI: 10.1109/TMAG.2010.2043347

[12] Babaei M, Faiz J, Ebrahimi BM, Amini S, Nazarzadeh J. A detailed analytical model of a salient-pole synchronous generator under dynamic eccentricity fault. IEEE Transactions on Magnetics. 2011;**47**:764-771. DOI: 10.1109/TMAG.2011.2105498

[13] Dorrel DG. Experimental behaviour of unbalanced magnetic pull in 3-phase induction motors with eccentric rotors and the relationship with tooth saturation. IEEE Transactions on Energy Conversion. 1999;**14**:304-309. DOI: 10.1109/60.790874

[14] Wei-li L, Tang L, Xiao-cheng Z, Jia-ming G. Calculation and analysis of high-speed permanent magnetic generator unilateral magnetic force. In: Proceedings of the 11th International Conference on Electrical Machines and Systems; Oct 17–20; Wuhan, China. 2008

[15] Lin W, Cheung RW, Ma Z-y, Jiang-jun R, Ying P. Finite-element analysis of unbalanced magnetic pull in a large hydro-generator under practical operations. IEEE Transactions on Magnetics. 2008;**44**:1558-1561. DOI: 10.1109/TMAG.2007.916023

[16] Joksimovic GM. Dynamic simulation of cage induction machine with air gap eccentricity. IEE Proceedings—Electric Power Applications. 2005;**152**:803-811

[17] Tabatabaei I, Faiz J, Lesani H, Nabavi-Razavi MT. Modeling and simulation of a salient-pole synchronous generator with dynamic eccentricity using modified winding function theory. IEEE Transactions on Magnetics. 2004;**40**:1550-1555. DOI: 10.1109/TMAG.2004.826611

[18] Faiz J, Ojaghi M. Unified winding function approach for dynamic simulation of different kinds of eccentricity faults in cage induction machines. IET Electric Power Applications. 2009;**3**:461-470. DOI: 10.1049/iet-epa.2008.0206

[19] Dorrell DG, Salah A. Detection of rotor eccentricity in wound rotor induction machines using pole-specific search coils. IEEE Transactions on Magnetics. 2015;**51**:1-4. DOI: 10.1109/TMAG.2015.2443711

[20] Sulla F, Svensson J, Samuelsson O. Symmetrical and unsymmetrical short-circuit current of squirrel-cage and doubly-fed induction generators. Electric Power Systems Research. 2011;**81**:1610-1618. DOI: 10.1016/j.epsr.2011.03.016

[21] Klontz KW, TJE M, MI MG, Karmaker H, Zhong P. Short-circuit analysis of permanent-magnet generators. IEEE Transactions on Industry Applications. 2011;**47**:1670-1680. DOI: 10.1109/TIA.2011.2154370

[22] Albright DR. Inter-turn short-circuit detector for turbine-generator rotor windings. IEEE Transactions on Power Apparatus and Systems. 1971;**PAS-90**:478-483. DOI: 10.1109/TPAS.1971.293048

[23] Fiser R, Lavric H, Bugeza M, Makuc D. FEM modeling of inter-turn short-circuits in excitation winding of turbo-generator. Przeglad Elektrotechniczny. 2011;**87**:49-52

[24] Li GJ, Hloui S, Ojeda J, Hoang E, Lecrivain M, Gabsi M, Zhu ZQ. Excitation winding short-circuits in hybrid excitation permanent magnet motor. IEEE Transactions on Energy Conversion. 2014;**29**:567-575. DOI: 10.1109/TEC.2014.2322194

[25] Shuting W, Yonggang L, Heming L, Guiji T. The analysis of generator excitation current harmonics on stator and rotor winding fault. In: IEEE International Symposium on Industrial Electronics; 9–13 July; Montreal, Que., Canada. 2006

[26] Wallin M, Lundin U. Dynamic unbalanced pull from field winding turn short circuits in hydropower generators. Electric Power Components and Systems. 2013;**41**:1672-1685. DOI: 10.1080/15325008.2013.835360

[27] Yonggang L, Guowei Z, Yucai W, Heming L. Impact of rotor inter-turn short-circuit on generator rotor force. Electrical Information and Mechatronics and Applications. 2012; **143-144**:125-131. DOI: 10.4028/www.scientific.net/AMM.143-144.125

[28] Ramirez-Nino J, Pascacio A. Detecting interturn short circuits in rotor windings. Computer Applications in Power, IEEE. 2001;**14**:39-42. DOI: 10.1109/67.954526

[29] Campbell SR, Kapler J, Sasic M, Stone GC. Detection of rotor winding shorted turns in turbine generators and hydrogenerators. In: Cigre 2010 Session; 22–27 August; Paris, France. 2010

[30] Biet M. Rotor faults diagnosis using feature selection and nearest neighbors rule: Application to a turbogenerator. IEEE Transactions on Industrial Electronics. 2013;**60**:4063-4073. DOI: 10.1109/TIE.2012.2218559

[31] Khezzar A, Kaikaa MY, El Kamel Oumaamar M, Boucherma M, Razik H. On the use of slot harmonics as a potential indicator of rotor bar breakage in the induction machine. IEEE Transactions on Industrial Electronics. 2009;**56**:4592-4605. DOI: 10.1109/TIE.2009.2030819

[32] Wu Q, Nandi S. Fast single-turn sensitive stator interturn fault detection of induction machines based on positive- and negative-sequence third harmonic components of line currents. IEEE Transactions on Industry Applications. 2010;**46**:974-983. DOI: 10.1109/TIA.2010.2045329

IntechOpen